Electrical Engineering
https://doi.org/10.1007/s00202-021-01273-x

ORIGINAL PAPER

Control of Grid Integrated Photovoltaic system using new Variable Step Size Least Mean Square adaptive filter

Avdhesh kumar[1] · **Rachana Garg**[1] · **Priya Mahajan**[1]

Received: 2 August 2020 / Accepted: 18 March 2021

Abstract
In this paper, a new variable step size least mean square adaptive filter-based control algorithm is proposed to generate reference current for voltage source converter of a grid-integrated PV system. The proposed control generates reference current by extracting the fundamental active and reactive component from load current with fast convergence. The proposed control offers better initial transients and dynamic performance than conventional LMS and synchronous reference frame-based control. Grid-integrated PV system is modelled in MATLAB/Simulink and is tested on different loading condition viz. nonlinear load, unbalanced load and variable load. Further, to validate the efficacy of the proposed control, it is also tested in real time on prototype hardware in the laboratory. It has been observed that proposed control provides compensation of harmonic and reactive power of the local load. Distortion at grid side of the system is within the limits as per IEEE-519 standard.

Keywords Variable step size least mean square (VSSLMS) · Power quality (PQ) · Voltage source converter (VSC)

1 Introduction

The nonlinear loads, viz. arc furnaces and variable frequency drives, etc., at consumer side have deteriorated the quality of power in utility grid. As a consequence, distribution system suffers from low power factor, unbalance current, poor voltage regulation, increase in neutral current, transients, harmonic distortion and flicker in distribution grid. To improve these power quality (PQ) issues, photovoltaic (PV) system has been integrated to a distribution grid. The main features of a PV system integrated to grid are: maintaining grid current sinusoidal by compensating the harmonics, neutralizing the effect of unbalance loads and maintaining power factor of the grid at unity [1–5]. To ensure the effectiveness of the proposed control, IEEE-519 standards are taken in to the consideration [6, 7]. As per IEEE-519, less than 5% total harmonic distortion (THD) in grid current and less than $\pm 5\%$ voltage fluctuations are allowable at PCC [7, 8]. Therefore, to maintain PQ within reasonable limits of IEEE requirements, it is necessary to establish an effective control of grid-integrated PV system with improved performance. PV system operated to get maximum efficiency using various algorithms [9–11]. Various conventional control algorithms of MPPT such as incremental conductance (INC), adaptive step size MPPT with single sensor and perturb & observe (P&O) are presented.

Many conventional control techniques viz. synchronous reference frame (SRF), unit template, least mean square (LMS) and least mean fourth (LMF) have been implemented [4, 7–17]. A phase locked loop (PLL) is required to transform three phases to synchronous frame in SRF-based control, but sometimes it shows computational delay and also it has to be tuned preceding to its operation. In the literature [18], PLL performance has been found to be easily influenced by distortions and noise and to overcome these drawbacks SOGI PLL has been proposed, but it also suffers

from poor dynamic response and uses generalized integrator thus requiring tuning of gains. Reference current is estimated using the voltage and current of the PCCC in the implementation of IRPT; therefore, fluctuation in voltage will reflect in the reference current. LMS and LMF suffer from fluctuations and less accuracy in estimating mean square error (MSE). In the past few decades, adaptive control algorithms have been proposed for many applications. Among them, the least mean square (LMS) algorithm is a distinguished one, whose stability and optimality are fully discussed in many literatures [13–20]. Due to its simplicity,

✉ Avdhesh kumar
iesavd@gmail.com

[1] Electrical Engineering Department, Delhi Technological University, Delhi, India

Published online: 15 April 2021

conventional LMS adaptive control has been implemented widely, but the performance is often unsatisfactory because of poor dynamic performance, due to compromise between tracking capability and accuracy in fixed step size.

In the conventional LMS adaptive control algorithm, estimation of mean square of error (MSE) is accomplished by fixed step size. Fixed step size (μ) is a positive scalar constant that governs the rate of convergence and stability of the algorithm. Step size (μ) value must be small and positive to maintain the stability of the adaptive filter. A trade-off point between the convergence rate and SME is an issue while choosing the value of the step size. The step size, used in most of these adaptive algorithms, is the function of a filtering error signal that is not equal to zero when the filter converges [21, 22, 23]. However, the characteristics of the error are responsible for deciding their step size. For further improvement, an improved new variable step size LMS (VSSLMS) control is proposed and implemented for grid integration of solar PV system in MATLAB/Simulink.

In this paper, a new variable step size LMS (VSSLMS) adaptive filter is derived by regulating the step size. The step size (μ) in proposed control merges estimation error, small positive constants α and β, respectively. Step size (μ) helps to reduce instantaneous estimation errors thus accelerating the convergence rate of the algorithm [21]. The purpose of the grid-integrated PV system using proposed control is to accomplish the load necessity, then after filling the load necessity, remaining power is supplied to the grid. Whenever, generated power is not enough and then load necessity is fulfilled by receiving extra essential power from the grid. The proposed algorithm successfully improves the initial transients and dynamic performance of the system with the faster convergence rate; hence, it decreases the error faster compared to the LMS and SRF. LMS and SRF controls show poor/slower convergence rate which reduces dynamic performance of the system. These challenges can be improved by proposed control. The proposed VSSLMS control algorithm is also implemented and tested in real time on prototype hardware in the laboratory.

The prime contributions of the paper are given below:

1. Proposed VSSLMS algorithm extracts active and reactive fundamental component from load current with a faster rate of convergence; hence, dynamic performance get improved.
2. PF of the grid has been improved by compensating the reactive power.
3. Maintains grid current to be sinusoidal and balanced during the nonlinear and unbalanced load, respectively, thus improves PQ.
4. It is more efficient than conventional LMS and SRF control due to faster tracking abilities during dynamic loading condition.
5. The proposed control is efficient under adverse scenario of the grid viz. unbalance and distorted grid voltage.

2 System description

Figure 1 demonstrates the proposed grid-integrated PV system. Proposed system consists of PV array, DC-DC boost converter, MPPT, VSC, interfacing inductors and various loads. To get the maximum efficiency from PV array, P&O MPPT is employed. Grid integration of PV system is accomplished using proposed VSSLMS adaptive control algorithm of VSC. Efficacy of the proposed algorithm is validated in MATLAB/Simulink and experimentally on a prototype hardware in the laboratory.

3 VSC Control technique

The proposed control algorithm is depicted in Fig. 2. Proposed control algorithm extracts the fundamental components from load current to estimate reference current. It improves the PQ of the grid by compensating harmonics. Performance of the system is analyzed in power factor correction (PFC) mode of operation. Grid-integrated PV system is modelled in MATLAB/Simulink2016 (a), and various system parameters are given in the appendix.

3.1 VSC switching pulse generation

3.1.1 Estimation of in-phase and orthogonal unit templates of voltages

The peak amplitude of voltage ($\mathcal{V}_t$) of grid voltage, can be calculated by:

$$\mathcal{V}_t = \sqrt{\frac{2}{3}\left(\mathcal{V}_{sa}^2 + \mathcal{V}_{sb}^2 + \mathcal{V}_{sc}^2\right)} \tag{1}$$

The in-phase unit template voltages ($\mathcal{U}_{pa}$,$\mathcal{U}_{pb}$, $\mathcal{U}_{pc}$) can be calculated from phase voltages ($\mathcal{V}_{sa}, \mathcal{V}_{sb}, \mathcal{V}_{sc}$) and peak amplitude of voltages ($\mathcal{V}_t$) [14] as follows:

$$\mathcal{U}_{pa} = \frac{\mathcal{V}_{sa}}{\mathcal{V}_t}, \mathcal{U}_{pb} = \frac{\mathcal{V}_{sb}}{\mathcal{V}_t}, \mathcal{U}_{pc} = \frac{\mathcal{V}_{sc}}{\mathcal{V}_t} \tag{2}$$

The reactive/orthogonal/quadrature unit templates ($\mathcal{U}_{pa}$,$\mathcal{U}_{pb}$, $\mathcal{U}_{pc}$) can be obtained from in phase unit template voltages as follows:

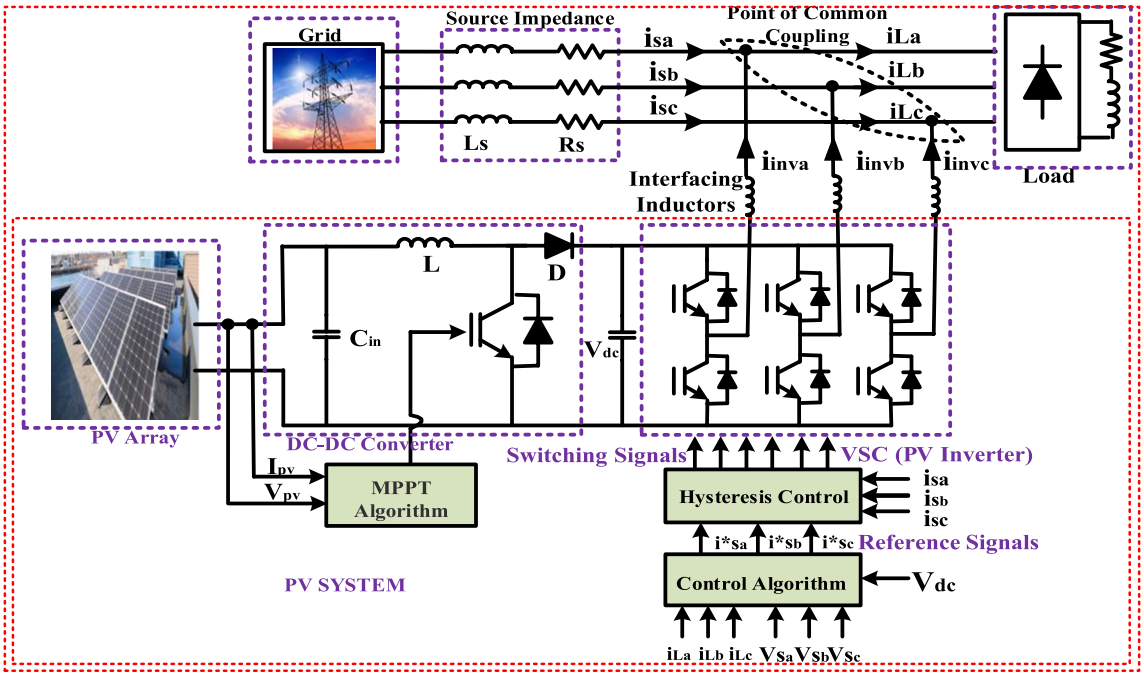

Fig.1 Proposed grid-integrated PV system

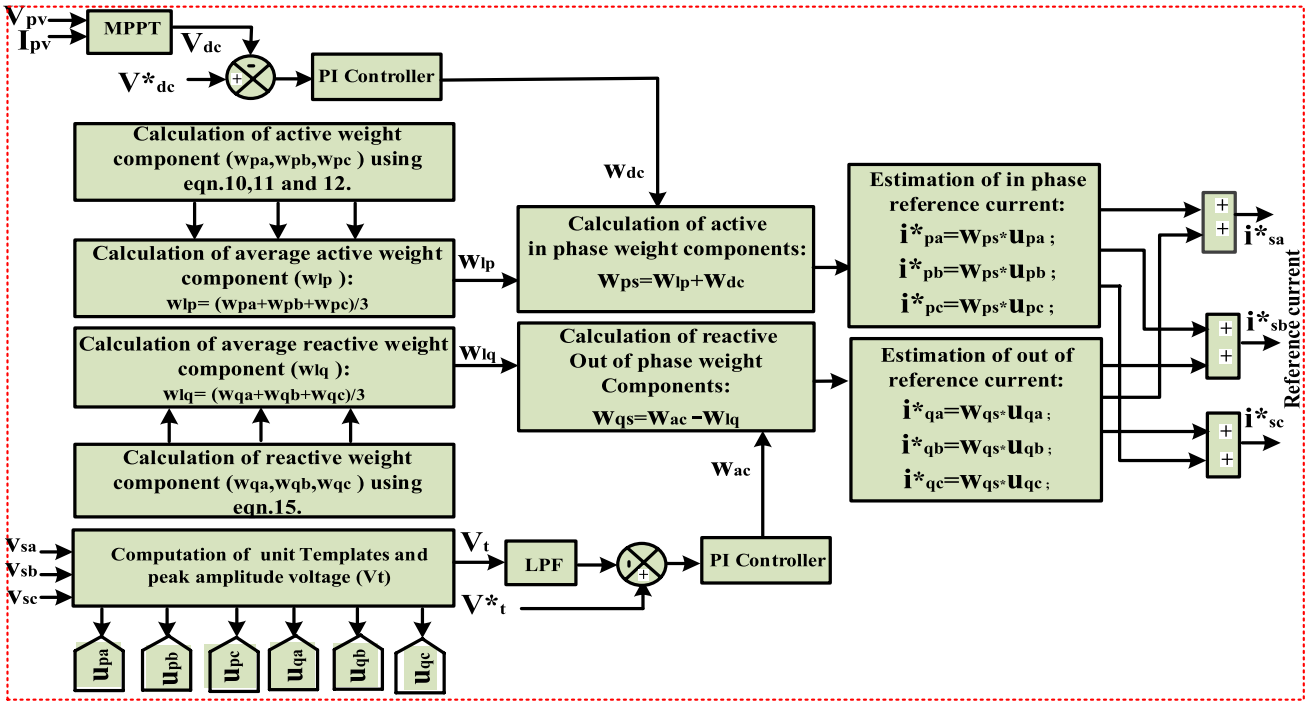

Fig.2 Proposed VSSLMS adaptive control for reference current generation

$$u_{qa} = -\frac{u_{pb}}{\sqrt{3}} + \frac{u_{pc}}{\sqrt{3}}; u_{qb} = \frac{\sqrt{3}u_{pa}}{2} + \frac{(u_{pb} - u_{pc})}{2\sqrt{3}};$$
$$u_{qc} = -\frac{\sqrt{3}u_{pa}}{2} + \frac{(u_{pb} - u_{pc})}{2\sqrt{3}} \tag{3}$$

3.1.2 Estimation of active and reactive weight components

Instantaneous estimation error (e_p) of active component in each phase at nth instant is estimated from in-phase unit template (u_p) and load current (i_L) for any phase "m" as follows:

$$e_{pm}(n) = i_{Lm}(n) - u_{pm}(n) * w_{pm}(n-1) \tag{4}$$

where w_p is fundamental active weights and "m" represents the phases "a", "b" and "c".

New variable step size (μ) for proposed control algorithm can be realized by mathematical equations [21, 23] as given below:

$$\mu(N) = \frac{\beta}{\{[1 + \exp(-\alpha|e(n)e(n-1)|)] - 0.5\}} \tag{5}$$

where e (n) represents the estimation error at nth instant.

Estimation error (e_p) of different phases e_{pa}, e_{pb}, e_{pc} is estimated using in phase unit template (u_p) and load current (i_L) at nth instant as follows:

$$e_{pa}(n) = i_{La}(n) - u_{pa}(n) * w_{pa}(n) \tag{6}$$

$$e_{pb}(n) = i_{Lb}(n) - u_{pb}(n) * w_{pb}(n) \tag{7}$$

$$e_{pc}(n) = i_{Lc}(n) - u_{pc}(n) * w_{pc}(n) \tag{8}$$

Fundamental active weights w_{pa}, w_{pb}, w_{pc} at $(n+1)$ instant for phase any phase "m" can be computed as:

$$w_{pm}(n+1) = w_{pm}(n) + \mu(n) * e_{pm}(n) \tag{9}$$

where $e_{pm}(n)$ is the priori estimation error and $\mu(n)$ is step size for minimum error. Updated weight vector $w_{pm}(n+1)$ is calculated from weight $w_{pm}(n)$ for overall error minimization. Updated weight vector for different phases given below:

$$w_{pa}(n+1) = w_{pa}(n) + \mu(n) * e_{pa}(n) \tag{10}$$

$$w_{pb}(n+1) = w_{pb}(n) + \mu(n) * e_{pb}(n) \tag{11}$$

$$w_{pc}(n+1) = w_{pc}(n) + \mu(n) * e_{pc}(n) \tag{12}$$

The fundamental active weight component of load (w_{lp}) is estimated by taking average of updated weight vector.

$$w_{\mathrm{lp}} = \frac{(w_{pa} + w_{pb} + w_{pc})}{3} \tag{13}$$

The purpose of proposed control technique is to minimize the error. Similarly, reactive component of error (e_q) and fundamental reactive weight components of load (w_{lq}) can be computed as follows:

$$e_{qm}(n) = i_{Lm}(n) - u_{qm} * w_{qm} \tag{14}$$

$$w_{\mathrm{lq}} = \frac{(w_{qa} + w_{qb} + w_{qc})}{3} \tag{15}$$

The error in sensed actual dc-link voltage (V_{dc}) as compared to (V^*_{dc}) reference voltage is compensated using PI controller. Output is dc loss weight (w_{dc}) of PI controller is given as:

$$w_{\mathrm{dc}}(n+1) = w_{\mathrm{dc}}(n) + K_{pd}\{v_{\mathrm{dc}(e)}(n+1) - v_{\mathrm{dc}(e)}(n)\} + K_{id}v_{\mathrm{dc}(e)}(n+1) \tag{16}$$

where K_{pd}, K_{id} are gains of dc bus PI controller. $v_{\mathrm{dc}(e)}(n+1)$ is the error of the sensed V_{dc} and V^*_{dc} dc bus voltage at $(n+1)$ th sampling time.

Total active weight (w_{ps}) component in reference current can be calculated as:

$$w_{\mathrm{ps}} = w_{\mathrm{lp}} + w_{\mathrm{dc}} \tag{17}$$

The active in-phase reference current components can be evaluated as:

$$i^*_{pa} = w_{ps} * \mathcal{U}_{pa};\ i^*_{pb} = w_{ps} * \mathcal{U}_{pb};\ i^*_{pc} = w_{ps} * \mathcal{U}_{pc} \tag{18}$$

The sensed peak magnitude of supply voltage is compared with set reference peak magnitude and generated error is compensated by PI controller. Output of the controller is ac loss weight (w_{ac}) is given as:

$$w_{\mathrm{ac}}(n+1) = w_{\mathrm{ac}}(n) + K_{pa}\{v_{te}(n+1) - v_{\mathrm{te}}(n)\} + K_{ia}v_{\mathrm{te}}(n+1) \tag{19}$$

where K_{pa}, K_{ia} are gains of ac voltage PI controller and $v_{\mathrm{te}}(n+1)$ is the error of the sensed ac voltage and reference ac bus voltage at $(n+1)$th sampling time.

Total reactive weight component (w_{qs}) of the reference current as shown below:

$$w_{\mathrm{qs}} = w_{\mathrm{ac}} - w_{\mathrm{lq}} \tag{20}$$

Reactive reference current components can be evaluated as:

$$i^*_{qa} = w_{qs} * \mathcal{U}_{qa};\ i^*_{qb} = w_{qs} * \mathcal{U}_{qb};\ i^*_{qc} = w_{qs} * \mathcal{U}_{qc} \tag{21}$$

3.1.3 Estimation of reference current and switching signal for VSC

The summations of reference active and reactive $\left(i^*_{pa},\ i^*_{pb},\ i^*_{pc}\right)$,$(i^*_{qa},\ i^*_{qb},\ i^*_{qc})$, respectively, are used to generate reference current $(i^*_{sa},\ i^*_{sb},\ i^*_{sc})$ which is given by:

$$i^*_{sa} = i^*_{pa} + i^*_{qa},\ i^*_{sb} = i^*_{pb} + i^*_{qb},\ i^*_{sc} = i^*_{pc} + i^*_{qc} \tag{22}$$

Further, reference current is compared with sensed grid current in hysteresis current controller for generation of gating signal for six switches of voltage source converter.

4 Simulation results and discussions

In the present section, simulation results have been presented. Performance of proposed new VSSLMS-based control of grid-integrated PV system is analyzed and compared with conventional SRF and LMS adaptive control. Proposed control maintains the current and voltage harmonics within limit of IEEE standard and reduces the reactive power burden on the grid.

Proposed control is modelled in MATLAB/Simulink environment and studied in PFC mode of operation. Simulation and experimental parameters of the system are given in the appendix.

4.1 Performance of grid-integrated PV system

4.1.1 Dynamic and Steady state behaviour under linear, nonlinear and unbalanced load at STC input

The performance of proposed new VSSLMS adaptive control under linear and nonlinear load depicted in Figs. 3 and 4, respectively. Various parameters of the system viz. V_{grid}, I_{grid}, I_{load}, I_{inv}, V_{dc} and power balance between grid, load and inverter are also analyzed.

It can be seen from Fig.3 that till 0.15 s PV inverter supplies 4kW active power and 3.0 kVAR of reactive demand of the load, Vgrid and Igrid are 180° out of phase (as excess 6.25 kW power is supplied to the grid), V_{dc} is maintained at 750V. The inverter alone supplies the load active and reactive power demand, which decreases the reactive power

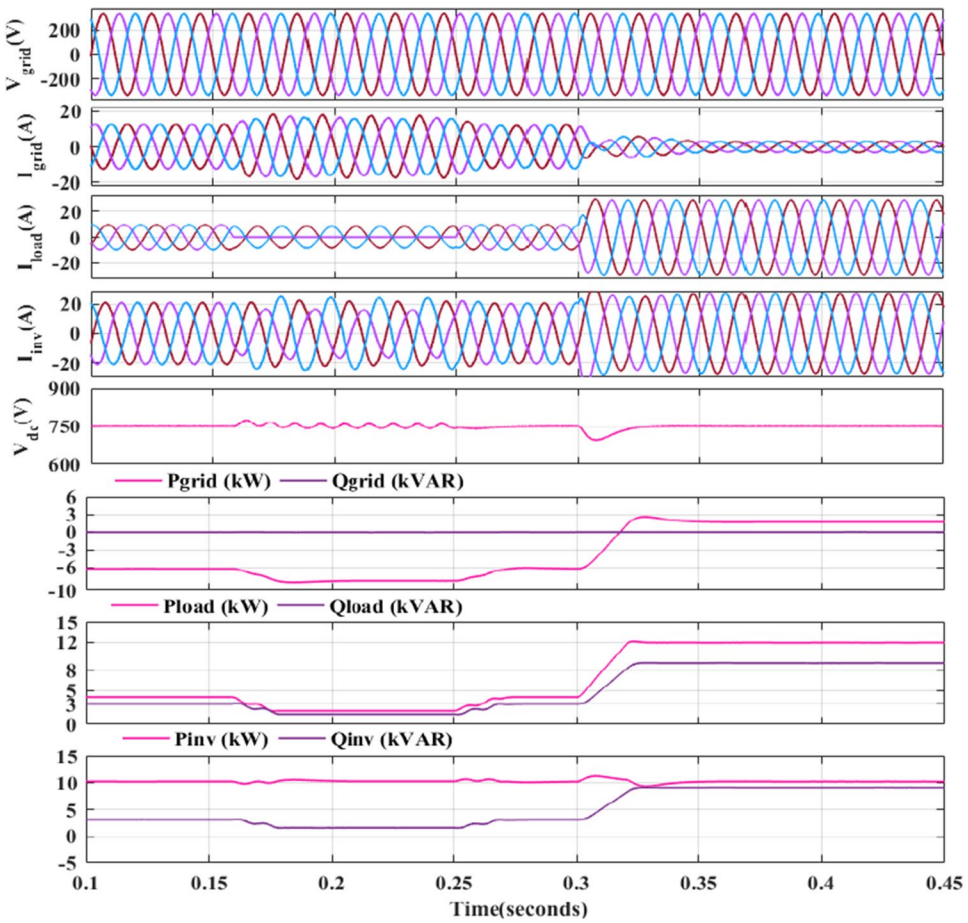

Fig. 3 Simulated performance of the system under linear (balance/unbalance) and variable load at STC

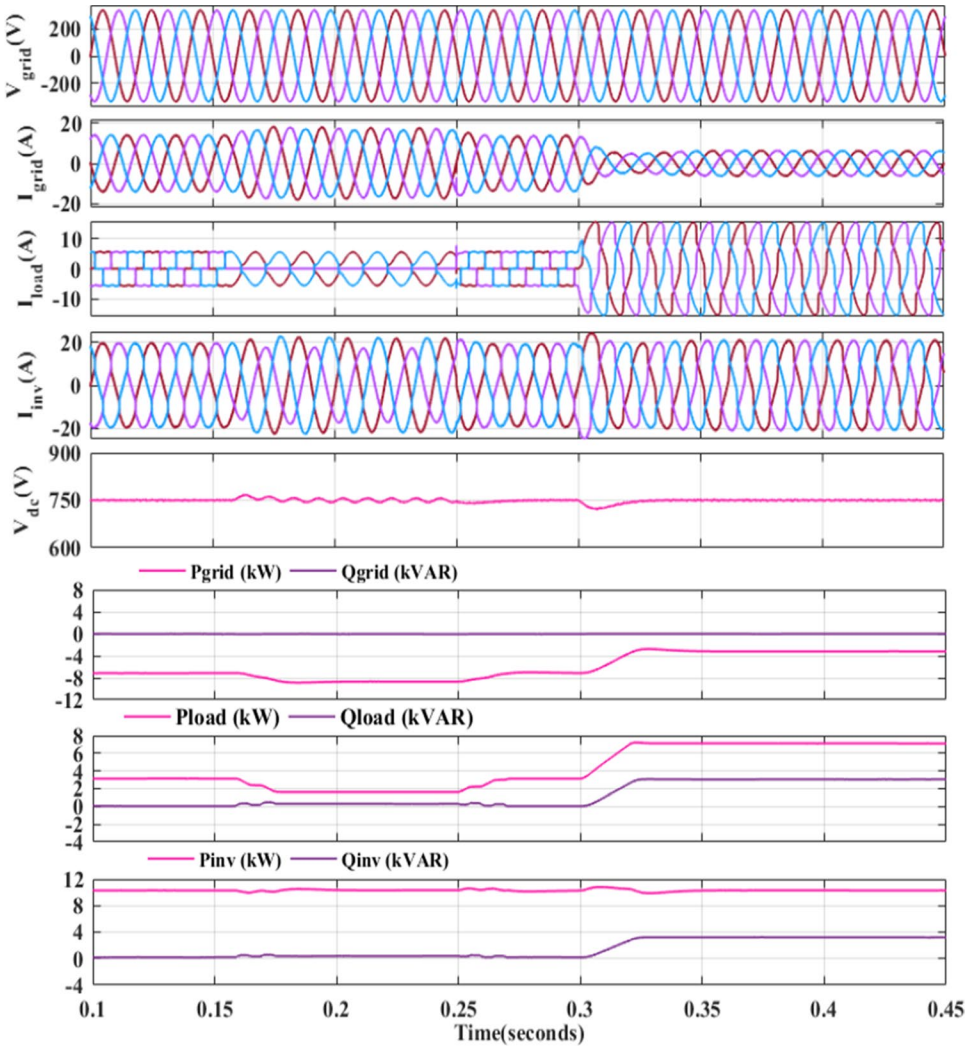

Fig. 4 Simulated performance of system under nonlinear (balance/unbalance) and load varying at STC input

drawn from the grid to zero, demonstrating that the proposed control is effective in maintaining the grid at UPF.

Further, unbalanced condition and load varying condition occur at 0.15 s and 0.30 s, respectively. Performance of the proposed control under linear unbalanced load condition by keeping one phase (phase *b*) disconnected between 0.15 and 0.25 s is studied and various parameters viz. V_{grid}, I_{grid}, I_{load}, I_{inv}, P_{grid}, Q_{grid}, P_{inv}, Q_{inv}, P_{load}, Q_{load}, and V_{dc} are analyzed and depicted in Fig. 3. During unbalance period, inverter current compensates, effect of load unbalance and maintains grid current to be balance. It also supplies the load requirement for reactive power and thus holds the grid at UPF along with the balance grid current. For the load varying condition between 0.3 and 0.45 s, an extra linear load of 10kVA, 0.8 pf lagging is added at 0.3 s in the system. After 0.3 s, load demand is 15kVA and 0.8 pf lagging (12 kW and 9 kVAR). Power supplied by PV inverter is 10.25 kW which is not enough to fulfill the load requirement, therefore, to meet the load demand extra required power 1.75 kW is taken from distribution grid.

It has been realised that during load variation and single phasing also that I_{grid} is sinusoidal and V_{dc} is maintained at 750 V. THD in I_{grid} is also maintained at 3.37% as depicted in Fig. 7a which is as per IEEE standard 519–2014, well within the limit.

Further, to test the proposed control under nonlinear load, it has been considered and results are shown in Fig. 4. It is observed that till 0.15 s PV system supplies its nominal power of 10.25 kW. It is observed from Fig. 4 that till 0.15 s V_{grid} and I_{grid} are 180° out of phase, maintains V_{dc} at 750 V, PV inverter supplies 3.1 kW active power demand of the load. Further, remaining 7.15 kW power of the PV system is supplied to the grid.

Further, proposed control under nonlinear unbalanced and load varying condition is also tested. Under nonlinear unbalanced load condition by one phase '*b*' of load disconnected between 0.15 and 0.25 s and various parameters viz. V_{grid}, I_{grid}, I_{load}, I_{inv}, P_{grid}, Q_{grid}, P_{inv}, Q_{inv}, P_{load}, Q_{load}, and V_{dc} are analyzed and presented in Fig. 4. During unbalance period, inverter current compensates, effect of

load unbalance and maintains balanced grid current. It also supplies the load requirement for reactive power and thus holds the grid at UPF along with the balance grid current.

For the load varying conditions between 0.3 and 0.45 s, an extra linear varying load of 5kVA, 0.8 pf lagging is added at 0.3 s in the system of existing nonlinear load. After 0.3 s, load demand is 7.1 kW and 3 kVAR, out of which 7.1 kW is supplied by PV inverter, as its generated power is 10.25 kW, after satisfying the load requirement, remaining power 3.15 kW is supplied to grid. It has been realised that during load variation and single phasing also grid current is sinusoidal and V_{dc} is maintained at 750 V. THD in I_{grid} is also maintained at 4.12% as depicted in Fig. 7b which is as per IEEE standard 519–2014, well within the limit.

4.1.2 Dynamic and steady state behavior under linear and nonlinear load at varying insolation

Further, the proposed new VSSLMS control is also tested at varying insolation under linear and nonlinear load. Solar irradiance is decreased at 0.15 s from 1000 to 700 W/m^2 and again increased to 1000 W/m^2 at 0.25 s; thus, solar PV current decreased; thus, PV output power is reduced and vice versa.

A 20kVA, 0.8 pf lag linear load is considered, simulated results and corresponding various parameters viz. V_{grid}, I_{grid}, I_{load}, I_{inv}, P_{grid}, Q_{grid}, P_{inv}, Q_{inv}, P_{load}, Q_{load}, and V_{dc} of the PV inverter are shown in Fig. 5. It is observed from Fig. 5, that both V_{grid} and I_{grid} are in phase (as power is supplied from grid to load), V_{dc} is maintained at 750 V, PV inverter supplies its generated power 10.25 kW which is not enough to fulfill the load demand of 20kVA, 0.8pf lag(16 kW and 12kVAR); therefore, to meet the load demand, extra power 5.75 kW is taken from distribution grid, while 12 kVAR

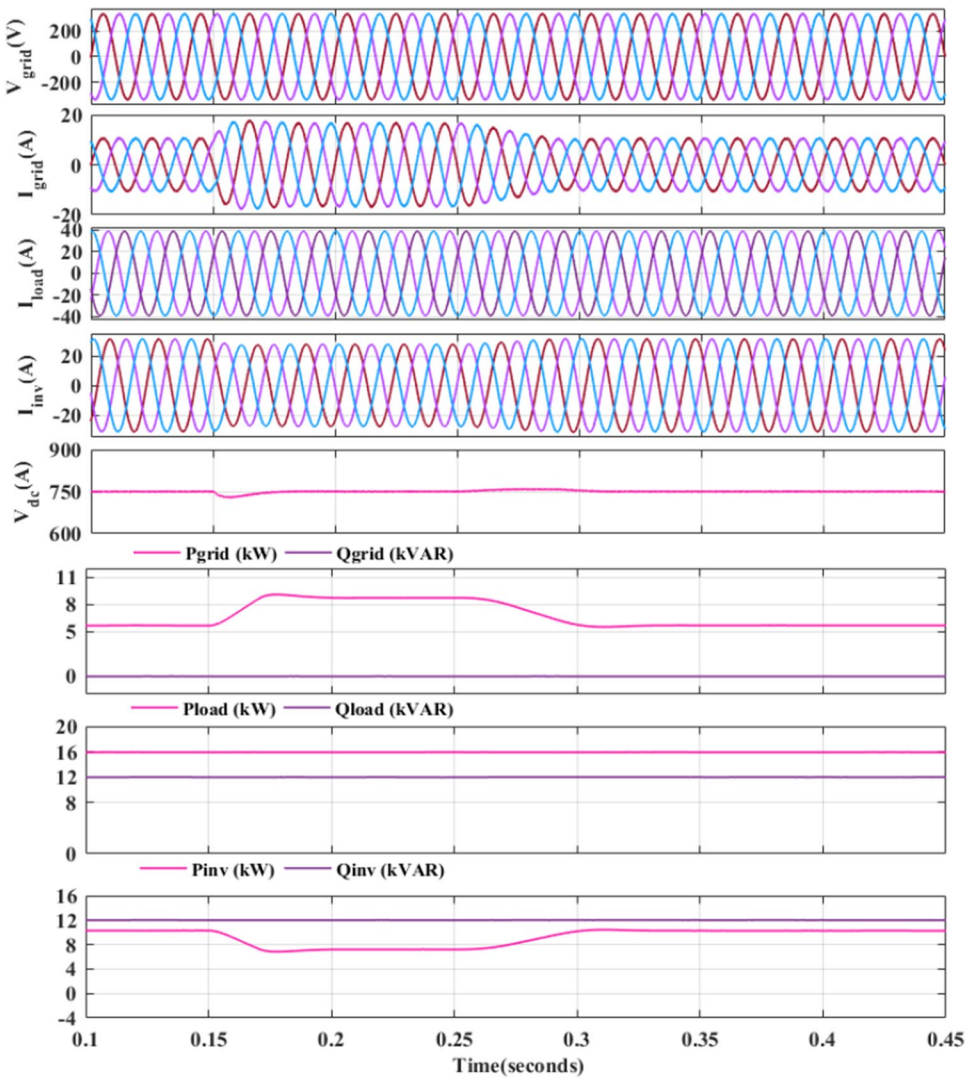

Fig. 5 Simulated performance of system under linear load at varying insolation

of reactive demand of the load is supplied by PV inverter alone, showing proposed control is efficient in maintaining the grid at UPF.

Further, the proposed algorithm on linear load is tested under varying insolation from 0.15 to 0.25 s. The performance of system using proposed algorithm under linear load condition under varying insolation between 0.15 and 0.25 s is analysed and various parameter viz. V_{grid}, I_{grid}, I_{load}, I_{inv}, P_{grid}, Q_{grid}, P_{inv}, Q_{inv}, P_{load}, Q_{load}, and V_{dc} are presented in Fig. 5. Due to decrease in solar insolation, P_{inv} is

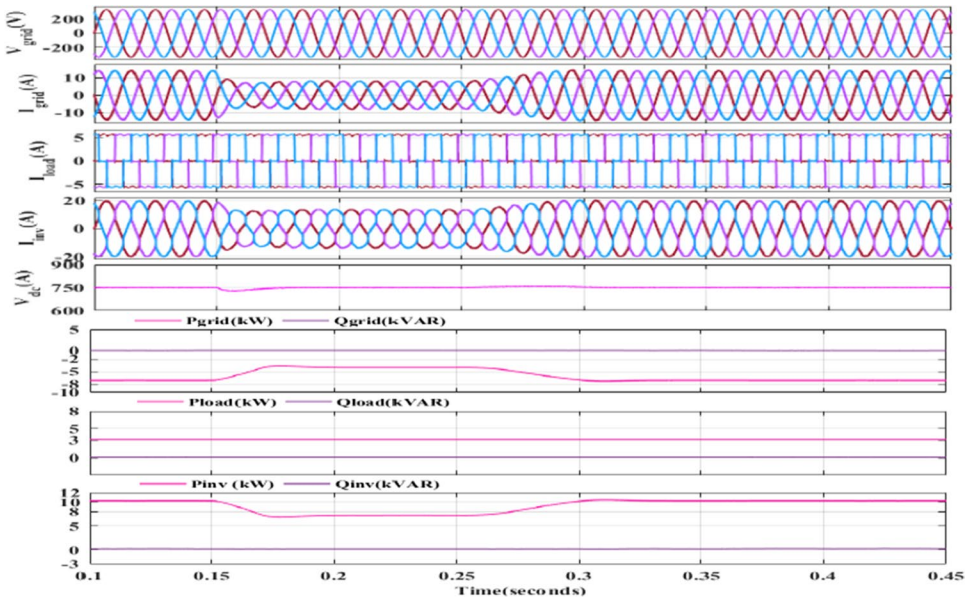

Fig. 6 Simulated performance of system under nonlinear load at varying insolation

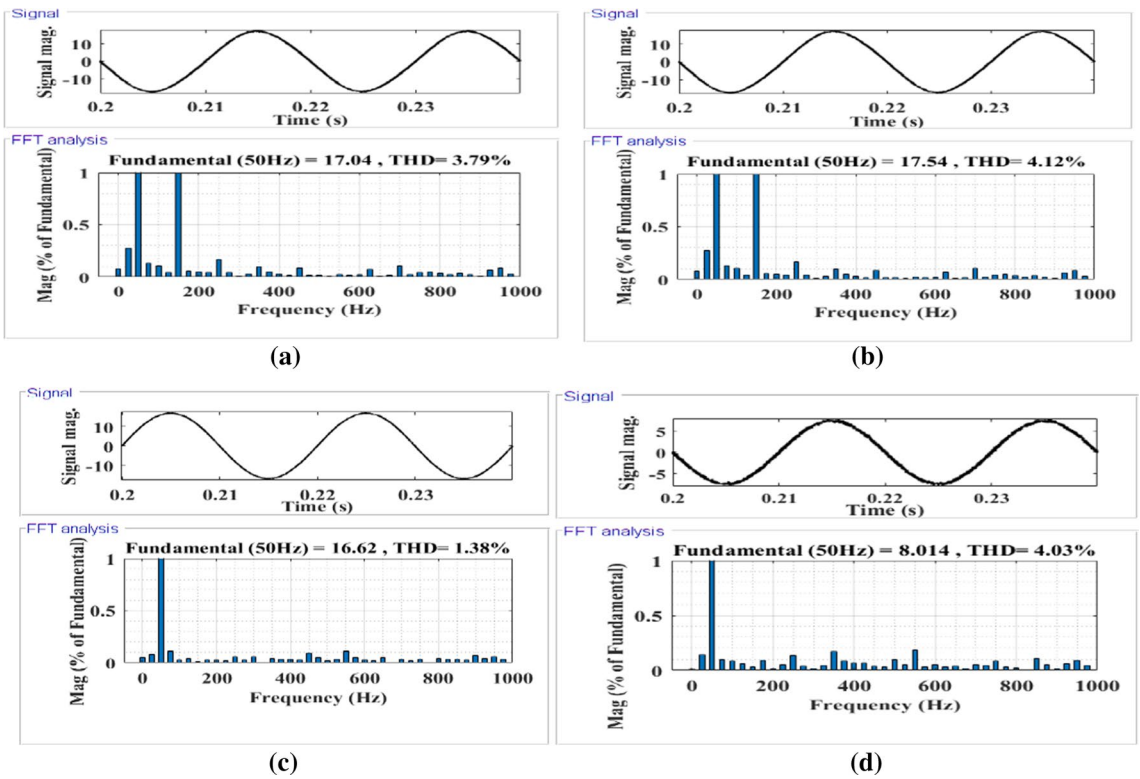

Fig. 7 **a**, **b** Compensated grid current waveform and THD under linear and nonlinear load, respectively, at STC; **c** and **d** compensated grid current waveform and THD under linear and nonlinear load, respectively, at varying insolation

decreased to 7.75 kW at 0.15 s causing the grid to supply 2.5 kW more power (total 8.25 kW) to the load as depicted in Fig. 5, while total reactive power demand of load is still supplied by inverter alone hence keeping grid at UPF during the adverse scenario of solar insolation. It has been observed that during solar insolation variation, sharing of active and reactive power between load (P_{load}, Q_{load}), grid (P_{grid}, Q_{grid}) and inverter (P_{inv}, Q_{inv}) is maintained, grid current is sinusoidal and maintains V_{dc} at 750 V. THD in I_{grid} is also maintained at 1.38% during the varying insolation also as shown in Fig. 7c which is as per IEEE standard 519–2014, well within the limit.

Further for a nonlinear load at varying irradiance, simulated results and corresponding various parameters viz. V_{grid}, I_{grid}, I_{load}, I_{inv}, P_{grid}, Q_{grid}, P_{inv}, Q_{inv}, P_{load}, Q_{load}, and V_{dc} of the PV inverter are shown in Fig. 6. V_{grid} and I_{grid} are out of phase by 180^0 (as power is supplied to grid), V_{dc} is maintained at 750 V, PV inverter supplies its generated power 10.25 kW after satisfying the load demand of 3.1 kW, rest power 7.15 kW is fed back to grid, while PV inverter alone supplying reactive power demand of the load, showing proposed control is efficient in maintaining grid at UPF.

After decrease in solar insolation, PV inverter power is decreased from 10.25 to 7.75 kW at 0.15 s leading to decrease in the power fed to the grid by 2.5 kW as shown in Fig. 6. While reactive power demand of load is supplied by PV inverter (VSC) alone hence keeping grid at UPF during the adverse scenario of solar insolation. After 0.25 s, insolation and PV power both have been increased and system remains in steady-state condition.

It has been observed that during solar insolation variation, active and reactive power is balanced between inverter (P_{inv},

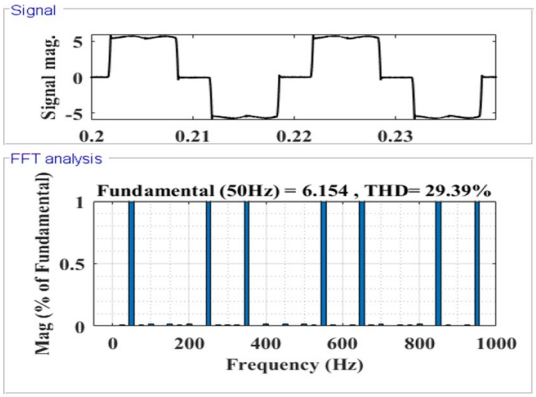

Fig. 8 Uncompensated nonlinear load current waveform and THD

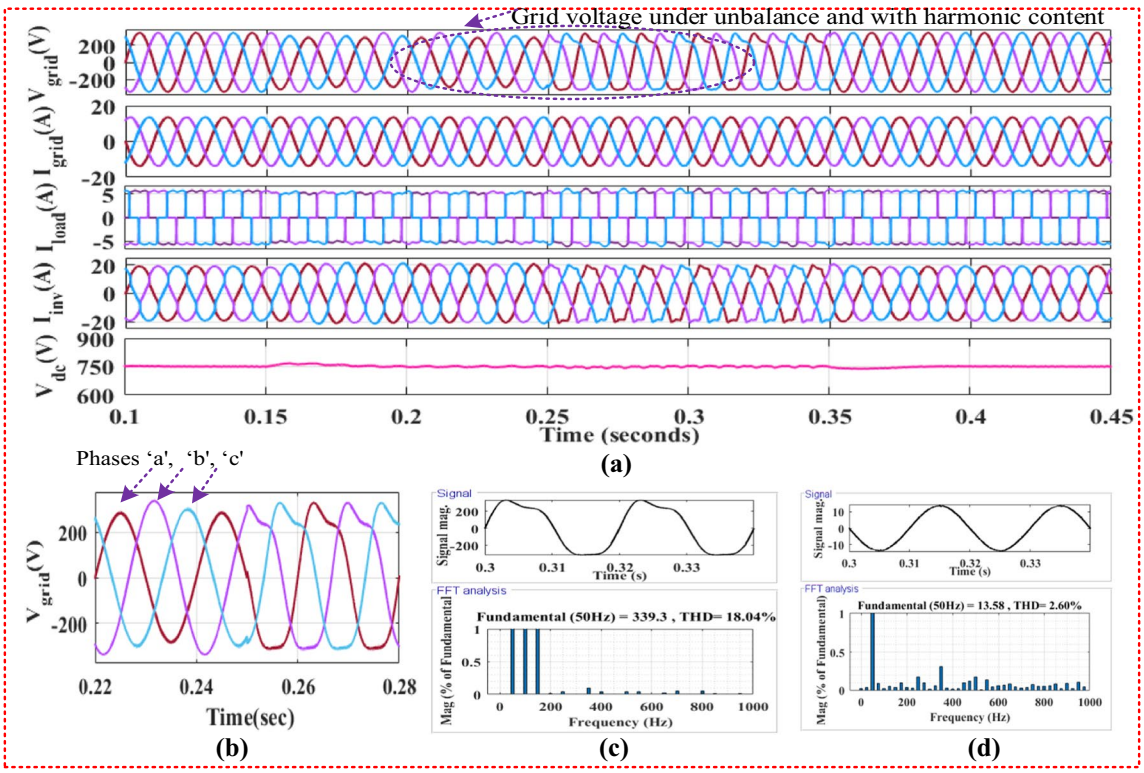

Fig. 9 **a** Performance with grid voltage under unbalance and grid voltage with harmonic content/distortion; **b** zoomed area of grid voltage waveform under unbalance and with harmonic content; **c** THD in grid current under grid voltage with harmonic content

Q_{inv}) load (P_{load}, Q_{load}) and grid (P_{grid}, Q_{grid}) is maintained, I_{grid} is sinusoidal and V_{dc} is maintained at 750 V. THD in I_{grid} is also maintained at 4.03% during insolation varying as shown in Fig. 7d, while load current THD is 29.39% as shown in Fig. 8.

4.1.3 Performance under unbalance grid voltage and grid voltage with harmonic contents

Further, proposed control is also tested under unbalanced grid voltage and grid voltage with harmonic content for nonlinear load. Figure 9 depicts the response of the system. Various parameters viz. V_{grid}, I_{grid}, I_{load}, I_{inv}, V_{dc} and THDs in grid voltage and current are analyzed and presented.

It can be seen from Fig. 9a that from 0.15 to 0.25 s, grid voltage is under unbalance and suffers from distortion between 0.25 and 0.35 s, respectively. During unbalance voltage of grid which is decreased by 16% and 12% of phases "*a*" and "*c*", respectively, as can be seen from Fig. 9a, b. Under unbalanced grid voltage condition, the proposed algorithm maintains grid current to be balanced and free from harmonics irrespective of voltage unbalance and load harmonics. It is also maintaining grid at UPF along with the balance grid current.

Further, the behaviour of the system is observed when grid voltage with harmonic content up to 18.4% THD as shown in Fig. 9c. During the adverse scenario of grid voltage with harmonic content, VSC maintains the THD in grid current as 2.6% as shown in Fig. 9d, which is within the IEEE standards. Hence, proposed control is efficient in maintaining grid current to be sinusoidal viz. free from harmonics and balanced irrespective of grid voltage harmonics and load harmonics as depicted in Fig. 9.

4.1.4 Comparison of proposed VSSLMS control and conventional SRF and LMS

Figure 10 shows comparison of proposed VSSLMS control with conventional SRF and LMS adaptive control. Nonlinear load viz. bridge rectifier with RL load ($R = 100\ \Omega$, 100 mH) is considered and further to investigate the transient response

Table 1 Comparison of proposed control with SRF and LMS control

Control algorithm	Settling time (sec)	Overshoot in active component (W_{ps})	Undershoot in active component (W_{ps})
SRF	0.06	160	− 58
LMS	0.05	140	− 50
Proposed	0.03	75	− 25

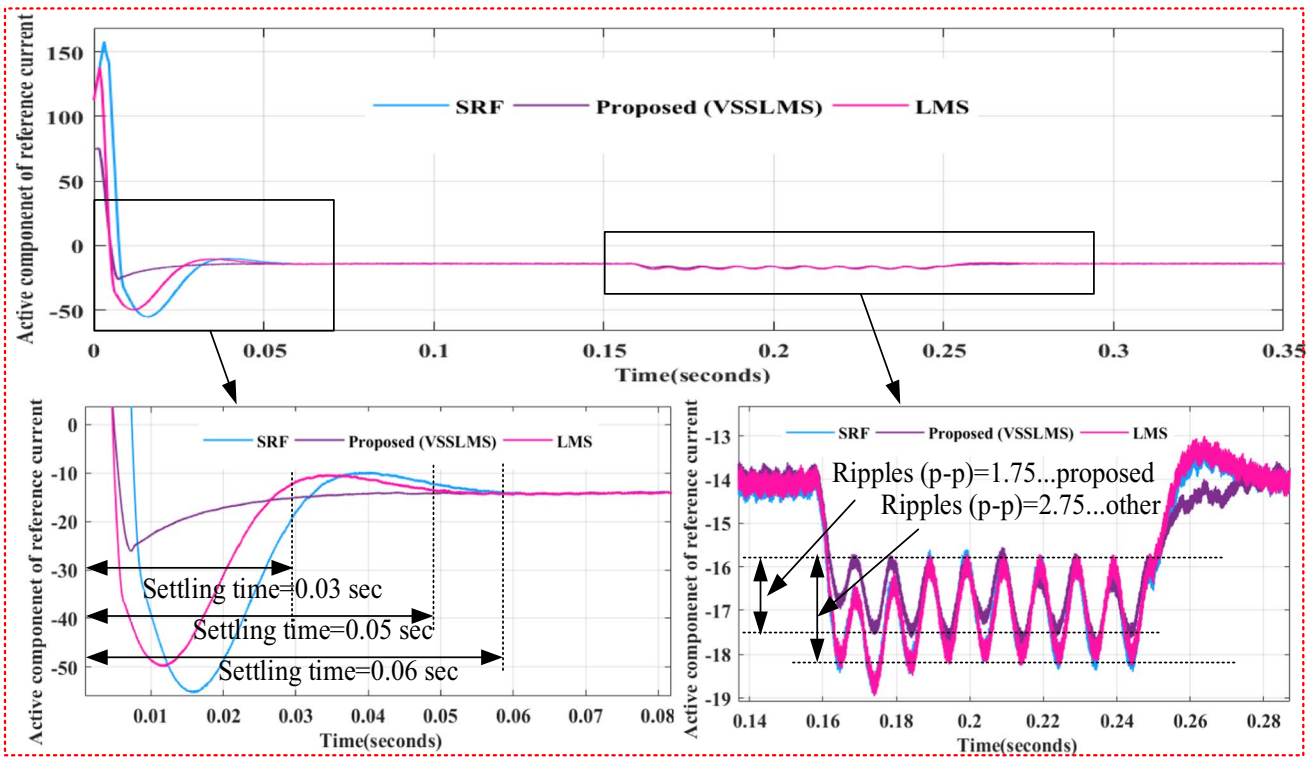

Fig. 10 Comparative performance of proposed control with SRF and LMS control

during load perturbation one phase of load is kept removed from 0.15 to 0.25 s.

It can be seen from Fig. 4 that till 0.30 s, PV system supplies its rated active power. It is observed that till 0.30 s V_{grid} and I_{grid} are 180° out of phase (as power is fed to the grid); therefore, active component of reference supply current is negative as it can be seen from Fig. 10.

Figure 10 shows the comparison of transient and dynamic performance under considered load. It can be seen from the Fig. 10 that during grid integration, proposed control gives best initial transient response in terms of settling time, overshoot and undershoot as given in Table 1 and has less oscillations. Further during load perturbation, it can be seen that proposed control has lower ripples as compared to that of the conventional SRF and LMS control, settling time using proposed VSSLMS control is 30 ms, whereas it's 50 ms and 60 ms, respectively, in case of conventional SRF and LMS. Hence, the proposed control is more efficient than that of other conventional SRF and LMS adaptive control.

5 Experimental Results

Due to limitation of the lab, developed prototype is made to operate as DSTATCOM by taking reference DC link voltage of 200V. Proposed control is tested to conduct VSC as a DSTATCOM. Figure 11 shows the prototype hardware setup developed in the laboratory.

Developed hardware has: 1. Grid, 2. interfacing indctors, 3. loads 4. power analyzer (Fluke/HIOKI-198), 5. inverter 6. DC supply, 7. DSO (Agilent made DSO7014A): Four-channel, 8. DSP-dSPACE-1202 MicroLabBox, 9.control desktop. Hall-effect-based sensors: voltage (LV 25-P) and current (LA 55-P).

5.1 Performance of proposed control under various load and grid conditions

5.1.1 Linear load

Performance of proposed control, under linear load of 0.48 kVA, 0.93 pf lagging has been considered. Various experimental parameters of the system viz. V_{grid}, I_{grid}, I_{load}, current supplied by inverter (I_{inv}) of one phase "a", before and after compensation are shown in Fig. 12a. Power factor of the load is 0.93 pf lagging, before compensation, it can be seen from Fig. 12b, while after compensation reactive power supplied by grid is approximately zero, showing UPF operation of proposed control as shown in Fig. 12c. After compensation, load reactive demand is fulfill by the VSC alone. Figure 12b and c show the power factor of the grid before and after compensation, respectively. Power factor of grid is maintained UPF after compensation as it can be seen from Fig. 12c as reactive power fed by grid zero.

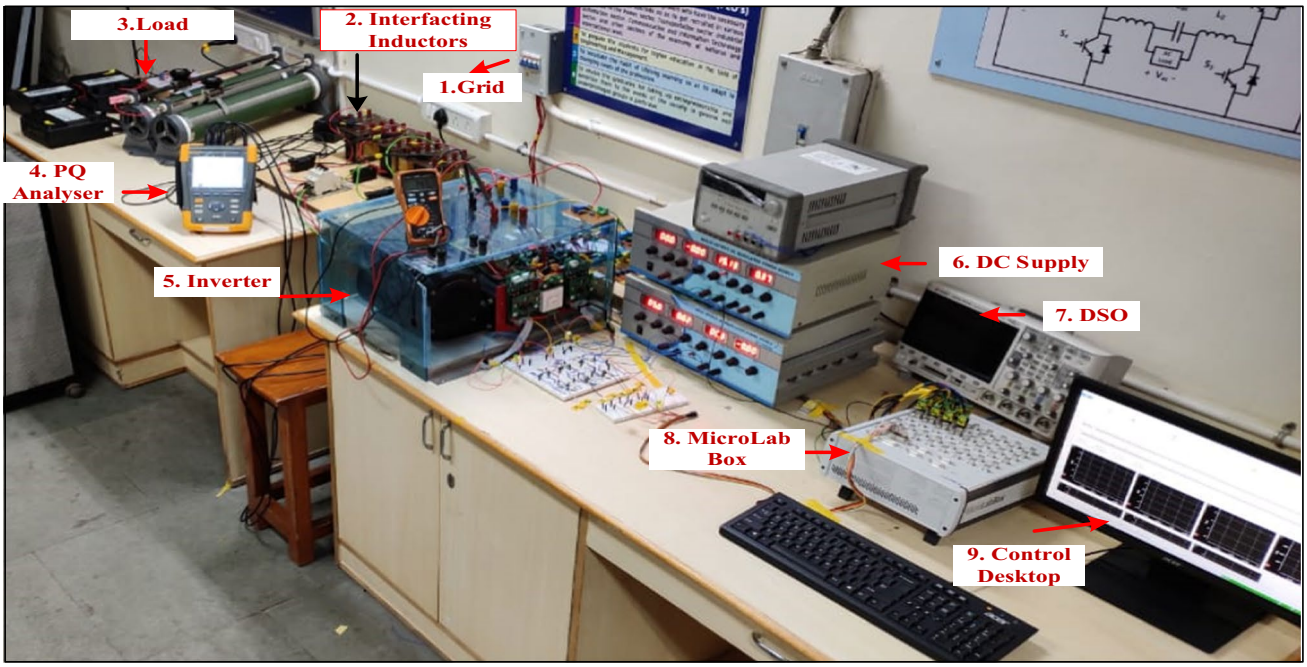

Fig. 11 Hardware prototype of DSTATCOM

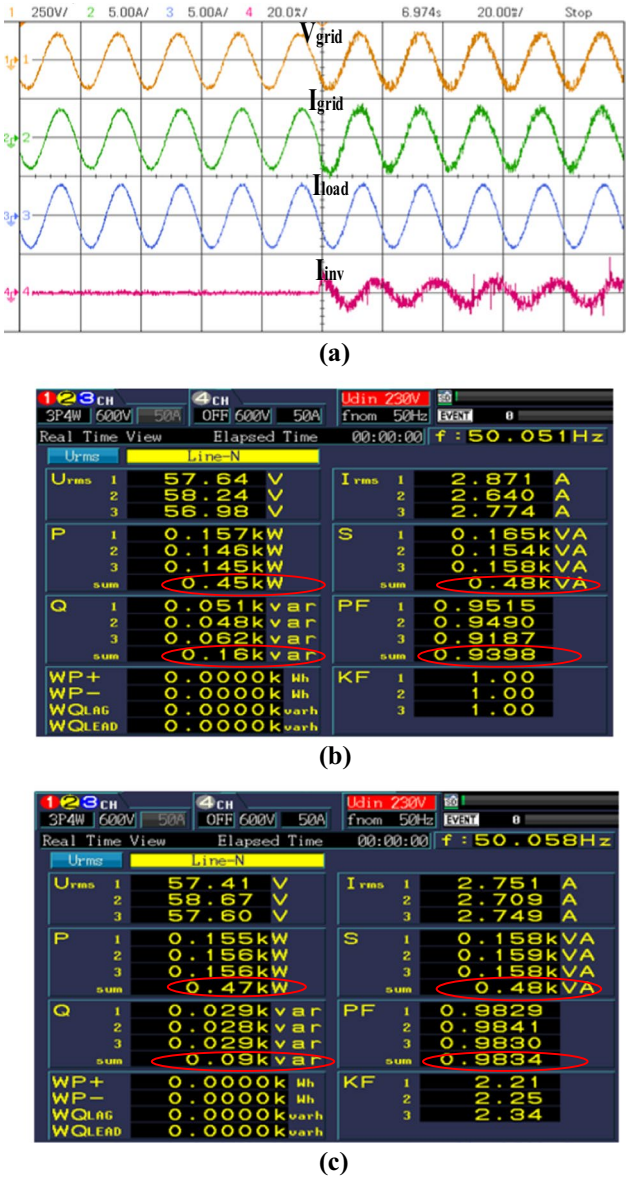

Fig. 12 Experimental result using proposed control under: **a** waveform; **b** and **c** load parameter and pf before and after compensation respectively

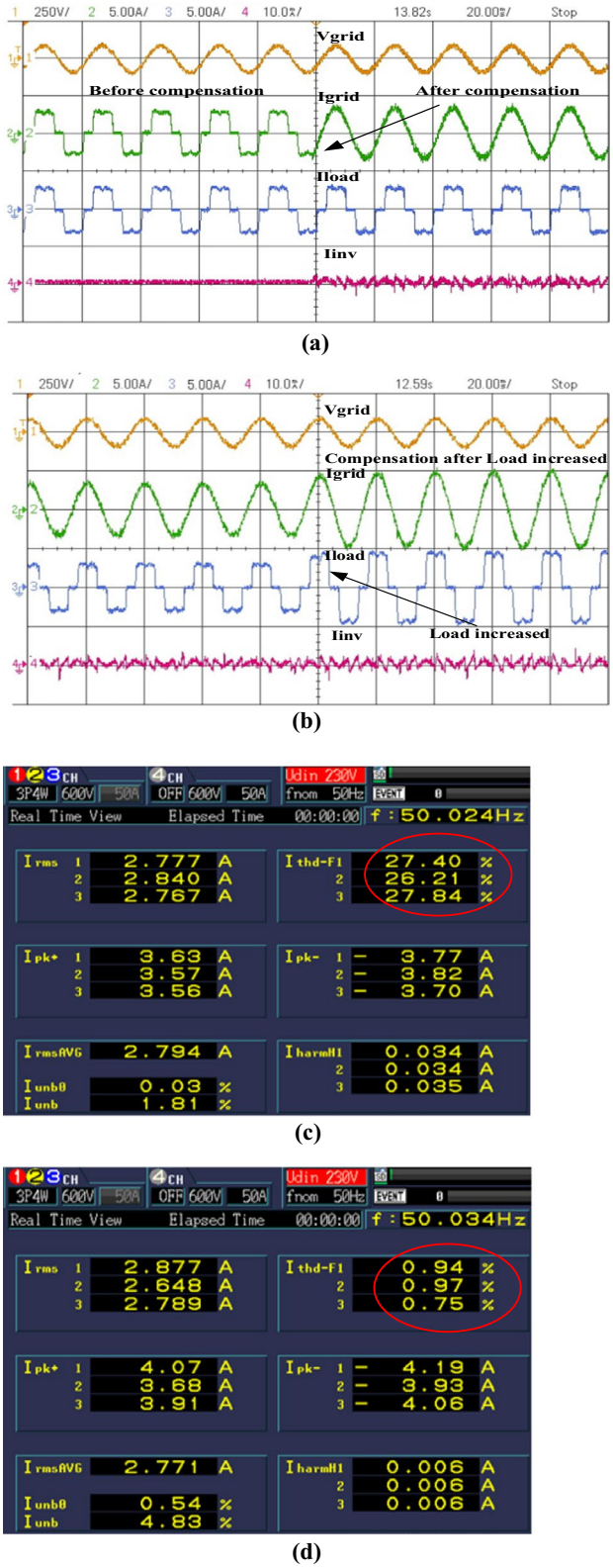

Fig. 13 Parameter under: **a** performance under nonlinear load; **b** performance under nonlinear load during load variation(increased); **c** THD in grid current before compensation under nonlinear **d** THD in grid current after compensation under nonlinear load

5.1.2 Nonlinear load

Performance of proposed control is tested on hardware prototype under nonlinear load by connecting a diode bridge rectifier with R load ($R = 50\ \Omega$). Figure 13a shows the V_{grid}, I_{grid}, I_{load}, current supplied by inverter (I_{inv}) respectively of one phase ('a') and Fig. 13b shows the load variation from 50 to 40 Ω. Inverter act as a harmonic compensator by compensating the harmonics of local loads. THD in grid current is less than 1%, while nonlinear load current THD is approximately 27% as shown Fig. 13c, d, respectively, which is well within IEEE standard 519–2014. It is analyzed that using

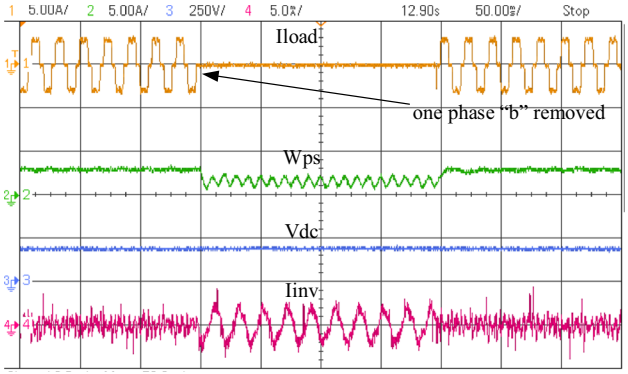

Fig. 14 Experimental result under nonlinear unbalance load

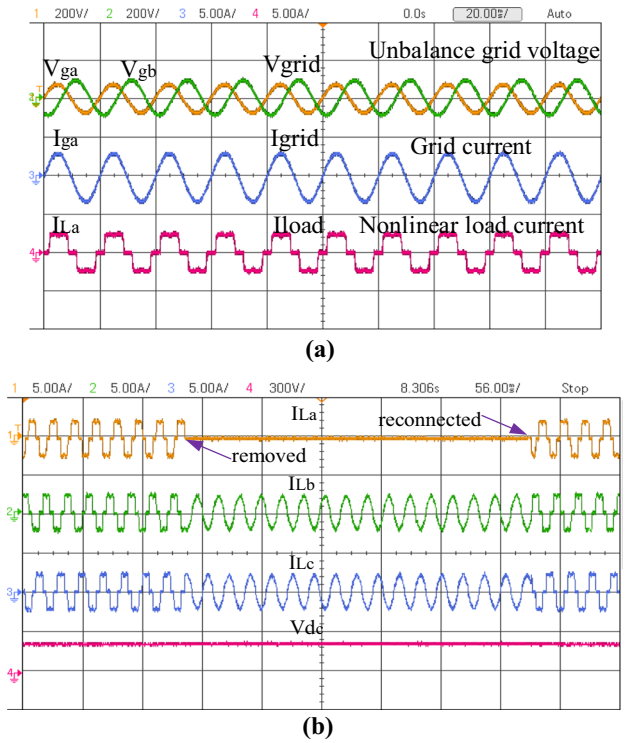

Fig. 15 Response of the system under unbalance grid voltage: **a** load under unbalance voltage of grid; **b** load unbalance

proposed control, grid current is improved significantly in terms of distortion by removing the harmonics.

5.1.3 Nonlinear unbalance load

To study the performance of proposed control under nonlinear unbalanced load, existing diode bridge rectifier with R load ($R = 50\ \Omega$) is taken. Unbalanced is created by removing one phase for few cycles and again connected back. Various experimental parameters of the system viz. I_{load}, fundamental active component (W_{ps}), V_{dc} and I_{inv} are shown

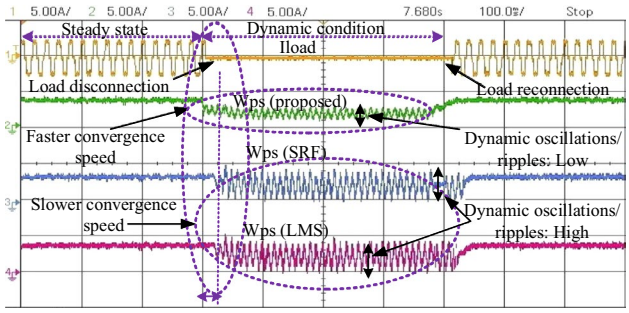

Fig. 16 Comparison of proposed and conventional SRF- and LMS-based control

Table 2 Comparison of proposed algorithm, conventional SRF and LMS

S.N	Criteria	SRF	LMS	Proposed
1	Accuracy	Good	Moderate	Better
2	Convergence	Slow	Moderate	Good
3	Complexity	High	Low	Low
4	Step size	NA	Constant	Variable
5	dSPACE-1202/sampling time	50 µS	40µS	40 µs
6	Filtering type	Time domain	Adaptive	Adaptive
7	Static error	High	High	Low
8	Dynamic oscillations in active component	High	High	Low

in the Fig. 14. From the experimental result, performance is efficient.

5.1.4 Performance under unbalance grid Voltage

Performance of proposed control is also tested under unbalance grid voltage at nonlinear and unbalanced load both. From Fig. 15a, it can be seen that, during the unbalance of voltage of the grid which is decreased by 17% (approx.) in phase '*a*', proposed control is efficient in maintaining the grid current to be balance and free from harmonics. Furthermore, during the unbalance of the load by means of removing one phase of load, different phases of load current are depicted in Fig. 15b. It has been found that performance using proposed control is efficient under unbalance scenario of the grid voltage also.

5.1.5 Comparison of proposed and conventional SRF and LMS based control

Performance of proposed VSSLMS control has been compared with conventional LMS and SRF control and is depicted in Fig. 16. It has been observed that proposed control's performance is efficient over other conventional

control and provide comparatively 40 ms faster convergence speed with minimum oscillations during dynamic condition viz. unbalanced load. Moreover, proposed control does not require any complex block like phase lock loop (PLL) for the synchronisation, which reduces the additional computational burden and provides faster response in terms of convergence speed compared to the SRF and LMS algorithm to estimate the reference current. Table 2 shows the comparative analysis of proposed control with other conventional control.

6 Conclusion

Solar PV system has been integrated to grid and has been studied using proposed new VSSLMS adaptive control algorithm of VSC. Proposed algorithm performance is tested at STC and varying insolation both under various balanced/unbalanced loads. Under various conditions, UPF operation of inverter is maintained and the THD in grid current is within the limits as per IEEE standards 519–2014. Proposed control is compared with conventional SRF and LMS adaptive control and it is found that proposed algorithm depicts better transient response under PV grid integration and dynamic load (unbalance) also. Proposed algorithm is validated experimentally in the laboratory on prototype hardware. Simulation and experimental investigations justify the efficacy of the proposed algorithm. Moreover, solar-PV system using proposed new VSSLMS adaptive control maintains the PQ of the system along with the PV power generation.

Appendix

Simulation parameters grid voltages (V_{sabc}): 415 V, frequency: 50 Hz, line impedances (R_s, L_s): 0.01 Ω, 0.1mH, interfacing inductor (L_f): 7mH, DC link capacitor (C_{dc}): 1000 µF, $V_{dc(ref)}$: 750 V; $\alpha = 20$; $\beta = 0.01$; sampling time (T_s) = 5.5 µs; source impedance:($R_s = 0.01$ Ω, $Ls = 0.1$ mH) per phase;

Solar PV parameters: nominal power:10.25 kW, nominal voltage: 410 V, nominal current: 25 A;

Boost converter parameters: L: 0.5 mH, switching frequency (f_s): 10 kHz, capacitor (C): 1000 µF, duty cycle (D): 0.43;

Various loads: linear load (balanced/unbalanced): 5 kVA, 0.8 pf lag (unbalanced between 0.15 and 0.25 sec); nonlinear load: bridge rectifier $R = 100$ Ω, $L = 100$mH (unbalanced between 0.15 and 0.25 sec); linear varying load: 5 kVA, 0.8 pf lag + 10 kVA, 0.8 pf lag (between 0.3 and 0.45 sec.); nonlinear varying load: (bridge rectifier $R = 100$ Ω, $L = 100$ mH) + 5 kVA, 0.8 pf lag (between 0.3 and 0.45 sec);

Experimental parameters of the prototype hardware: grid voltage ($V_{L\text{-}L}$) = 100 V(58 V/phase); reference dc link voltage ($V_{dc(ref)}$) = 200 V; VSC rating = 25 kVA; interfacing inductor (L_f) = 5 mH; nonlinear load ($R = 50$ Ω, 30 Ω); linear load: 0.48 kVA (0.93 pf lag); $\alpha = 20$; $\beta = 0.01$; gain of dc PI controller: $k_p = 0.50$, $k_i = 0.1$; $T_s = 40$ µs.

References

1. Verma P, Garg R, Mahajan P (2020) Asymmetrical interval type-2 fuzzy logic control based MPPT tuning for PV system under partial shading condition. ISA Trans 100:251–263. https://doi.org/10.1016/j.isatra.2020.01.009
2. Gupta N, Garg R (2017) Tuning of asymmetrical fuzzy logic control algorithm for SPV system connected to grid. Int J Hydrog Energy 42(26):16375–16385. https://doi.org/10.1016/j.ijhydene.2017.05.103
3. IEEE Std 1547:2003, IEEE standard for interconnecting distributed resources with electric power systems, IEEE Std 1547–2003, vol. 2014, pp. 1–16, 2003. https://doi.org/10.1109/IEEESTD.2003.94285
4. Choi W, Lee W, Han D, Sarlioglu B (2018) New configuration of multifunctional grid-connected inverter to improve both current-based and voltage-based power quality. IEEE Trans Ind Appl 54(6):6374–6382. https://doi.org/10.1109/TIA.2018.2861737
5. Trishan E, Patrick LC (2007) Comparison of photovoltaic array maximum power point tracking techniques. IEEE Trans Energy Convers 22(2):439449. https://doi.org/10.1109/TEC.2006.874230
6. Jiang Y, Qahouq JAA, Haskew TA (2012) Adaptive step size with adaptive-perturbation-frequency digital MPPT controller for a single-sensor photovoltaic solar system. IEEE Trans Power Electron 28(7):3195–3205. https://doi.org/10.1109/TPEL.2012.2220158
7. Shukl P, Singh B (2019) Grid integration of three-phase single-stage PV system using adaptive Laguerre filter based control algorithm under nonideal distribution system. IEEE Trans Ind Appl. https://doi.org/10.1109/tia.2019.2931504
8. Beniwal N, Hussain I, Singh B (2019) Second-order volterra-filter-based control of a solar PV-DSTATCOM system to achieve lyapunov's stability. IEEE Trans Ind Appl 55(1):670–679. https://doi.org/10.1109/TIA.2018.2867324
9. Liang X, Andalib-Bin-Karim C (2018) Harmonics and mitigation techniques through advanced control in grid-connected renewable energy sources: a review. IEEE Trans Ind Appl 54(4):3100–3111. https://doi.org/10.1109/TIA.2018.2823680
10. Beniwal N, Hussain I, Singh B (2018) Implementation of the DSTATCOM with an i-PNLMS-based control algorithm under abnormal grid conditions. IEEE. https://doi.org/10.1109/TIA.2018.2846739
11. Yang Bo, Li W, Zhao Yi, He X (2009) Design and analysis of a grid-connected photovoltaic power system. IEEE Trans Power Electron 25(4):992–1000. https://doi.org/10.1109/tpel.2009.2036432
12. Kanavaros D, Oriti G, Julian AL (2020) Novel implementation and comparison of active and reactive power flow control methods in a single phase grid-connected microgrid. IEEE Trans Ind Appl 56(2):1631–1639. https://doi.org/10.1109/tia.2020.2965080
13. Kazmierkowski MP (2015) Power quality: problems and mitigation techniques. IEEE Ind Electron Mag 9(2):62

14. Singh B, Chandra A, Al-haddad K Power quality problems and mitigation techniques. Wiley Online Library, ISBN: 978-1-118-92205-7
15. Barik PK, Shankar G, Sahoo PK (2019) Power quality assessment of microgrid using fuzzy controller aided modified SRF based designed SAPF. Int Trans Electr Energy Syst. https://doi.org/10.1002/2050-7038.12289
16. Singh B, Jayaprakash P, Kothari DP, Chandra A, Al Haddad K (2014) Comprehensive study of dstatcom configurations. IEEE Trans Ind Inform 10(2):854–870. https://doi.org/10.1109/TII.2014.2308437
17. Singh B, Shahani DT, Verma AK (2012) Power balance theory based control of grid interfaced solar photovoltaic power generating system with improved power quality. In: PEDES 2012—IEEE international conference on power electronics, drives and energy systems, pp. 1–7. https://doi.org/10.1109/PEDES.2012.6484359
18. Yada HK, Murthy MSR (2017) An improved control algorithm for DSTATCOM based on single-phase SOGI-PLL under varying load conditions and adverse grid conditions. In: IEEE international conference on power electronics, drives and energy systems. PEDES 2016, vol. 2016, pp. 1–6. https://doi.org/10.1109/PEDES.2016.7914564
19. Zeb K, Uddin W, Khan MA, Ali Z, Ali MU, Christofides N, Kim HJ (2018) A comprehensive review on inverter topologies and control strategies for grid connected photovoltaic system. Renew Sustain Energy Rev 94:1120–1141. https://doi.org/10.1016/j.rser.2018.06.053
20. Patel SK, Arya SR, Maurya R (2017) Harmonic mitigation technique for DSTATCOM using continuous time LMS adaptive filter. In:IEEE Uttar Pradesh section international conference on electrical, computer and electronics engineering. UPCON 2016, pp. 19–24. https://doi.org/10.1109/UPCON.2016.7894617
21. Huang HC, Lee J (2012) A new variable step-size NLMS algorithm and its performance analysis. IEEE Trans Signal Process 60(4):2055–2060. https://doi.org/10.1109/TSP.2011.2181505
22. Li Z, Li D, Xu X, Zhang J (2019) New normalized LMS adaptive filter with a variable regularization factor. J Syst Eng Electron 30(2):259–269. https://doi.org/10.21629/JSEE.2019.02.05
23. Yuan Z, Songtao X (2017) New LMS adaptive filtering algorithm with variable step size. In: Proceedings of the international conference on vision, image and signal processing. ICVISP 2017, pp. 1–4. https://doi.org/10.1109/ICVISP.2017.11